J. Fluid Mech. (1983), *vol.* 133, *pp.* 147–160
Printed in Great Britain

The reflection of obliquely incident tsunamis

By GEORGE F. CARRIER AND CLAUDE F. NOISEUX
Division of Applied Sciences, Harvard University

(Received 19 August 1982 and in revised form 24 January 1983)

When a tsunami is incident on a plane shelf, the waveform and amplitude of the reflected wave differ significantly from those of the incident wave, and, when the shelf has the extremely irregular character of real continental shelves, the contrast between the two amplitudes is even greater. Here we quantify these statements and we also give an account of the manner in which the run-up depends on the obliquity and on other parameters characterizing the incident wave.

1. Introduction

When a tsunami impinges obliquely on a large land mass with an irregular boundary the reflected wave will differ in waveform and in amplitude from the incident wave. In discussions of such matters, the *dissipation* associated with the reflection dynamics is frequently cited as the cause of the discrepancy between incident and reflected amplitudes. For a large tsunami with its very large characterizing lengthscales, however, it seem unlikely that frictional dissipation can account for much attenuation, and we present here analyses which suggest that the distorted and attenuated reflection is the result of both the 'phase mixing' which is intrinsic to frictionless reflection from an irregular shelf *and* to the more orderly distortion associated with the frictionless reflection from a plane shelf. The latter, for normal incidence, is implicit in earlier studies, but we are not aware that, as yet, the implications have been presented explicitly.

When a large tsunami travels a large distance (say M) across the Pacific, dispersion can play an important role in the evolution of the wave shape and amplitude but only for waves whose lateral scale is less than 50 miles or so and only over travel distances L of a few thousands of miles (Carrier 1971). The travel distance associated with the reflection process is much smaller than M, and, accordingly, one can analyse the phenomenon of interest here with a non-dispersive formulation of the gravity-wave dynamics.

Accordingly, we will adopt the classical linear shallow-water theory and treat three (families of) problems with it. In particular, we will find:

(1) the reflection of a given incident wave from a plane shelf;

(2) the ensemble average of the further distortion of that reflected wave by a stochastically characterized irregularity in the shelf boundary;

(3) the deterministic modification of an outcoming wave by a deterministic undulation in the shelf boundary; this third result will provide the basis for an argument that the stochastic result can be applied to *each* realization of the wave-with-ragged-boundary problem at sufficiently great offshore distances.

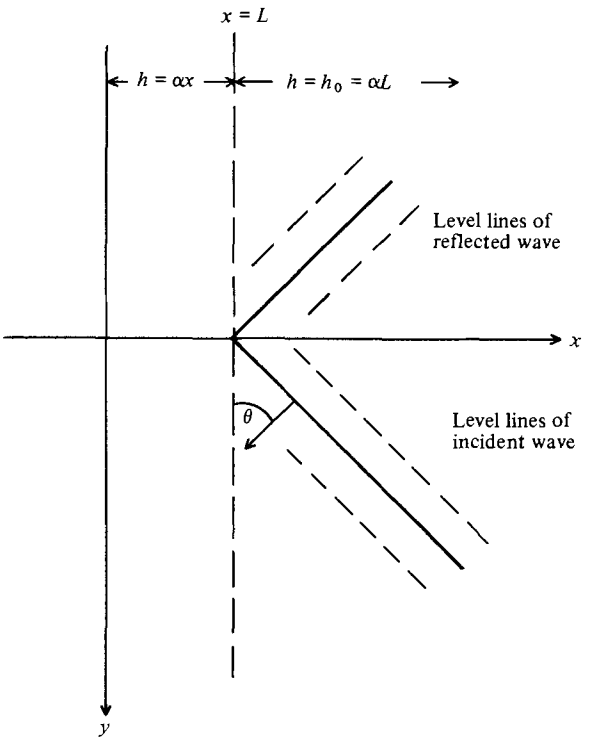

FIGURE 1. Geometry of wave problem. In the dimensionless coordinates of our analysis $L = 1$ and $\alpha = 1$; h is the depth of the shelf and h_0 is the uniform deep-water depth.

2. Reflection from a plane shelf

The conservation laws in the linear shallow-water approximation lead to

$$(h(x)\,\eta_x)_x + h(x)\,\eta_{yy} - \frac{1}{g}\eta_{tt} = 0, \tag{2.1}$$

where $h(x)$ is the water depth, x is distance seaward from the zero-depth line and η is the wave height. We confine our attention to waves that depend on y (distance parallel to the shore) and on t only in the combination

$$s = y - \frac{(gh_0)^{\frac{1}{2}}t}{\cos\theta},$$

where θ defines the obliquity with which the incident wave approaches the shelf (for normal incidence $\theta = \frac{1}{2}\pi$). The geometry is depicted in figure 1. In particular, the depth $h(x)$ is given by

$$h(x) = \begin{cases} \alpha x & (x \leqslant L), \\ \alpha L & (x \geqslant L). \end{cases}$$

When x and s are measured in units of shelf width, (2.1) becomes

$$\phi_{xx} - \tan^2\theta\,\phi_{ss} = 0 \quad (x > 1), \tag{2.2}$$

$$(x\eta_x)_x + (x - \gamma^2)\,\eta_{ss} = 0 \quad (x < 1), \tag{2.3}$$

where ϕ is just the name that we give η in the deep water (i.e. in $x > 1$) and $\gamma = \sec\theta$.

We seek solutions of (2.2) and (2.3) such that η includes a prescribed incident wave

and a reflected wave which is to be found. At the shelf edge we require that

$$\phi(1,s) = \eta(1,s), \tag{2.4}$$

$$\phi_x(1,s) = \eta_x(1,s). \tag{2.5}$$

The foregoing, including the prescription of ϕ_{inc}, suffice to determine ϕ and η uniquely.

When we invoke the use of the Fourier transform

$$\bar{\phi}(x,\xi) = \int_{-\infty}^{\infty} \mathrm{e}^{-\mathrm{i}\xi s}\,\phi(x,s)\,\mathrm{d}s,$$

(2.2) and (2.3) become

$$\bar{\phi}_{xx} + \xi^2 \tan^2\theta\,\bar{\phi} = 0 \quad (x > 1), \tag{2.6}$$

$$(x\bar{\eta}_x)_x - \xi^2(x-\gamma^2)\,\bar{\eta} = 0 \quad (x < 1). \tag{2.7}$$

The solution of (2.6) can be written in the form,

$$\bar{\phi} = \bar{A}(\xi)\,\mathrm{e}^{-\mathrm{i}\xi(x-1)\tan\theta} + \bar{B}(\xi)\,\mathrm{e}^{\mathrm{i}\xi(x-1)\tan\theta}, \tag{2.8}$$

and the first term is the transform of the incident wave. More precisely, the incident wave is

$$\phi_{\text{inc}} = A(\lambda), \tag{2.9}$$

where

$$\lambda = s - (x-1)\tan\theta.$$

The most general solution of (2.7) that is bounded at $x = 0$ is

$$\bar{\eta}(x,\xi) = C(\xi)\,\mathrm{e}^{-\xi x}\,M(\tfrac{1}{2}(1-\gamma^2\xi), 1, 2\xi x). \tag{2.10}$$

Here M is the confluent hypergeometric function (Abramowitz & Stegun 1965) defined by

$$M(a,1,z) = \sum_{n=0}^{\infty} \frac{a_n z^n}{(n!)^2}$$

where

$$a_n = a(a+1)\ldots(a+n-1). \tag{2.11}$$

It is also true (with $p = 2\xi x$ and $a = \frac{1}{2}(1-\gamma^2\xi)$) that

$$\bar{\eta}'(x) = C(\xi)\,\xi\,\mathrm{e}^{-\xi x}\,[2M_p(a,1,p) - M(a,1,p)], \tag{2.12}$$

which may be written (Abramowitz & Stegun 1965)

$$\bar{\eta}'(x) = \xi C(\xi)\mathrm{e}^{-\xi x}\,[M(a,1,p) - (1+\xi\gamma^2)\,M(a,2,p)].$$

It follows from (2.4), (2.5), (2.8), (2.10) and (2.12) that $\bar{B}/\bar{A}$ (the reflection coefficient) is given by

$$\frac{\bar{B}b(\xi)}{\bar{A}(\xi)} = \frac{1 - \mathrm{i}\dfrac{\psi}{\chi}\cot\theta}{1 + \mathrm{i}\dfrac{\psi}{\chi}\cot\theta}, \tag{2.13}$$

where

$$\psi = M(a,1,2\xi) - (1+\xi\gamma^2)\,M(a,2,2\xi),$$

$$\chi = M(a,1,2\xi),$$

It also follows that

$$\bar{\eta}(x,\xi) = \bar{A}(\xi)\,\mathrm{e}^{-\xi(x-1)}\,\frac{2}{\chi + \mathrm{i}\psi\cot\theta}\,M(a,1,2\xi x). \tag{2.14}$$

The information needed to invert numerically the Fourier transforms $\bar{\eta}(x,\xi)$ and $\bar{B}(\xi)$ is readily available (Abramowitz & Stegun 1965 and Appendix A) and we have

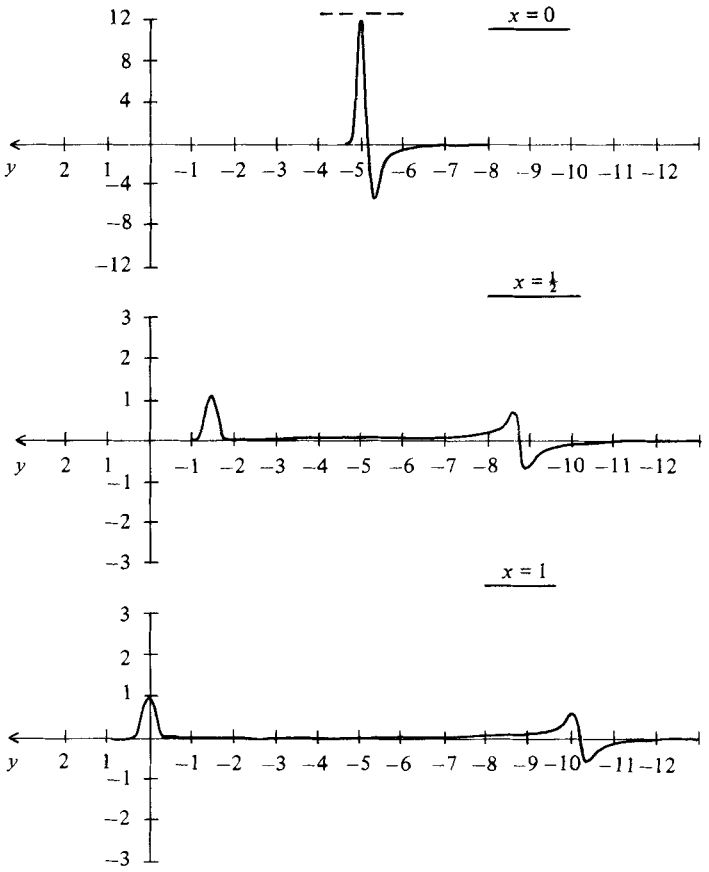

FIGURE 2. Wave profiles on the plane shelf with $w = 0.0625$, $\theta = \frac{3}{8}\pi$.

carried out the process for incident waves of the form†

$$A(\lambda) = \exp\left(-\frac{\lambda^2 \cos^2\theta}{w^2}\right)$$

at $x = 0, \frac{1}{2}, 1$, for each of the cases $w = 0.0625, 0.125, 0.25$ and 0.5 and $\theta = \frac{1}{2}\pi, \frac{1}{4}\pi, \frac{3}{8}\pi$.

The profiles of η *vs.* y plotted in figure 2–6 illustrate the major features of the computed results. The figures correspond to the time such that the crest of the incident wave passes through $x = 1$, $y = 0$. Note that the reflected wave (as well as the run-up $y(0, s)$) has, in each case, a dipole character (despite the one-signed incident wave), and that, for some parameters, there are artifacts of multiple reflection (see figure 6 at $y \approx -5$).

Several persistent trends are evident in the graphs. In figure 2 an additional profile at $x = \frac{1}{2}$ is included to show the general character of the waveform distribution across

† Analytically, it is very convenient to use a Gaussian as the generic waveform. It is clear that any smooth wave profile can be approximated by a linear combination of such waves, and its one-signed character is an especially useful reference point against which to compare the reflected waveform. The same building block played an equally useful role in the tsunami generation and propagation analysis (Carrier 1971), but for rather different mathematical reasons. In both instances, however, the underlying *justification* rests in each case on the fact that only the longer wavelength contributions to the waves are particularly important.

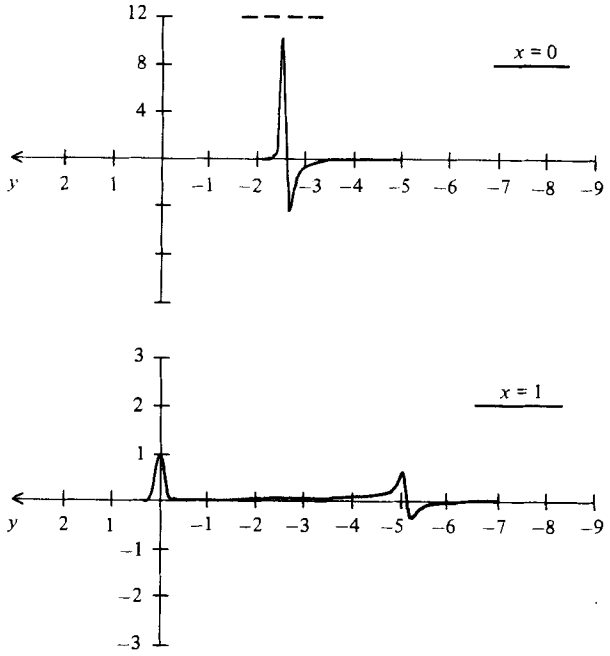

FIGURE 3. Wave profiles on the plane shelf with $w = 0.0625$, $\theta = \frac{1}{4}\pi$.

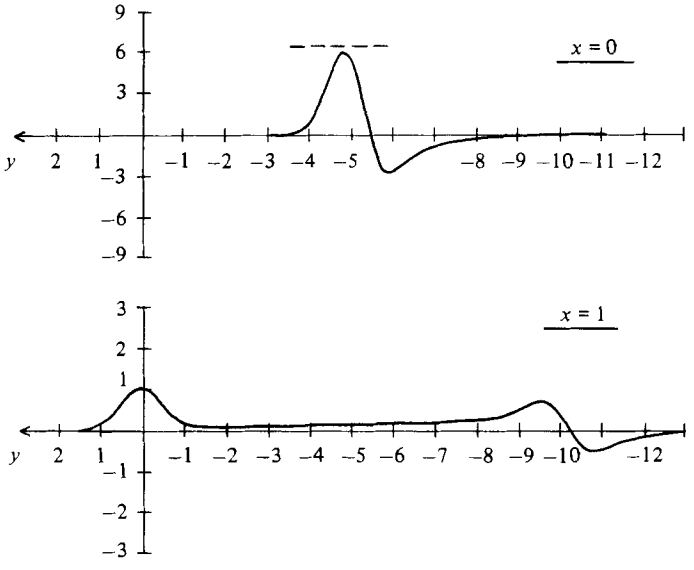

FIGURE 4. Wave profiles on the plane shelf with $w = 0.25$, $\theta = \frac{3}{8}\pi$.

the shelf – this example being representative of all the computed results. Also, the maximum run-up $\eta_m(0, s)$ at the shore occurs as normal incidence is approached (compare figures 2 and 3) and the value of $\eta_m(0, s)$ when $\theta = \frac{1}{2}\pi$ is shown in the figures by a dotted line. Furthermore, when the width of the incident pulse is decreased, $\eta_m(0, s)$ is increased and the dipole character of the reflected wave is enhanced. Note that, although a plot of η *vs.* y at fixed t would be meaningless for $\theta = \frac{1}{2}\pi$, the plot of η *vs.* y for $\theta = \frac{3}{8}\pi$ is an excellent approximation to a plot of η *vs.* t for $\phi = \frac{1}{2}\pi$.

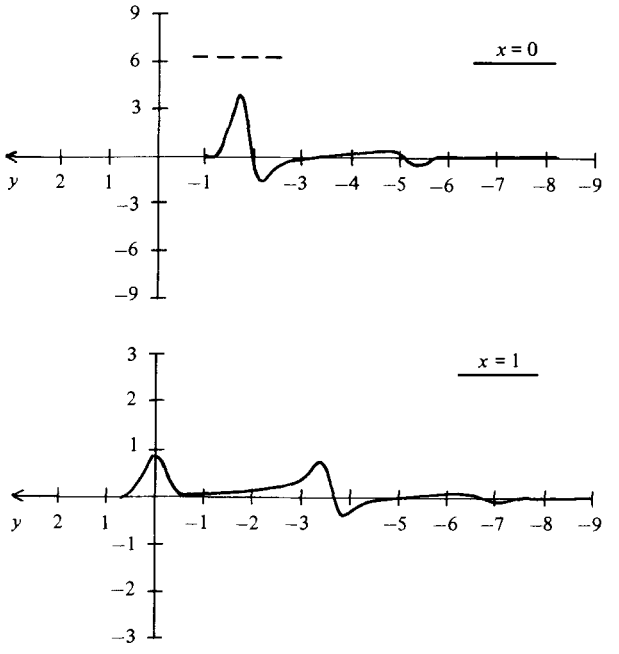

FIGURE 5. Wave profiles on the plane shelf with $w = 0.25$, $\theta = \frac{1}{8}\pi$.

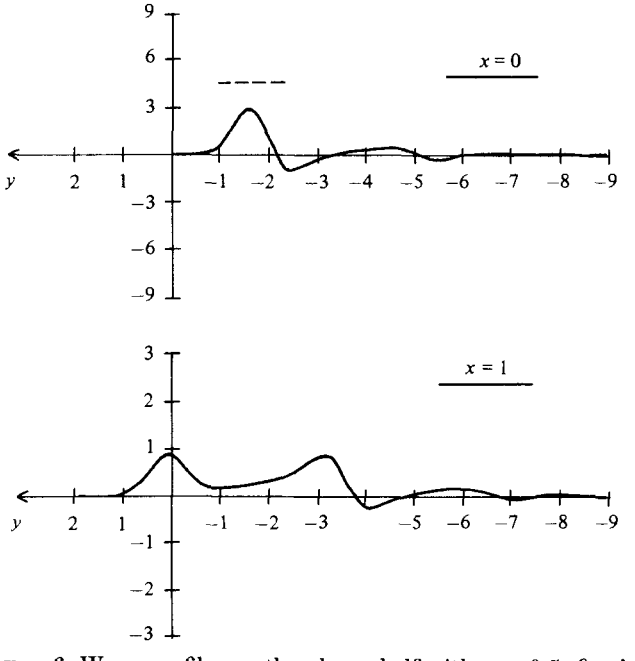

FIGURE 6. Wave profiles on the plane shelf with $w = 0.5$, $\theta = \frac{1}{8}\pi$.

It is of interest to note that the results are rather different when one adopts for the shelf geometry a constant depth that is smaller than h_0 in $0 < x < 1$ joined discontinuously to the deep water (h_0) at $x = 1$. A concise account of that problem is given in Appendix B. Note that there is *no* shelf level for which the results provide a reasonably good approximation to those for the sloping shelf.

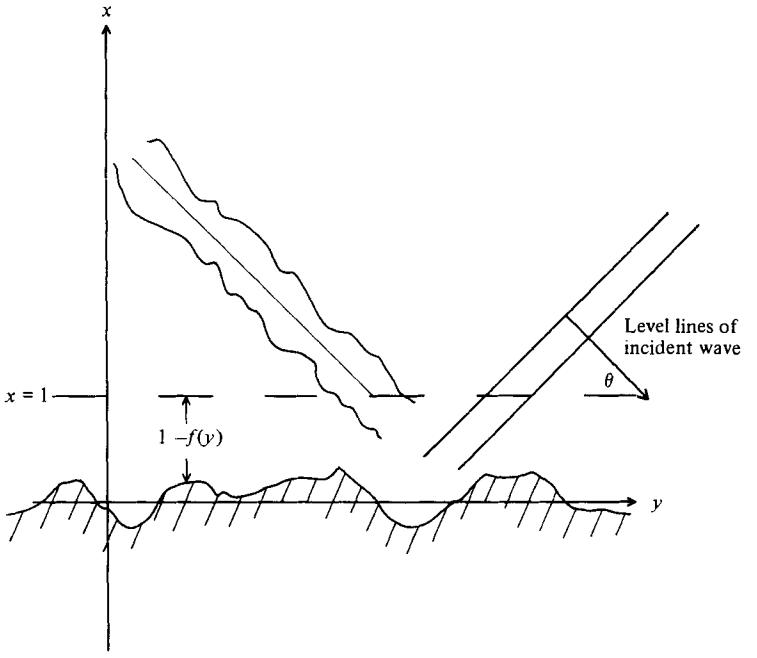

FIGURE 7. Schematic diagram of the ragged boundary given by $x = f(y)$, two constant-height profiles of the incident wave (solid lines) and an artistic rendition of the analogues characteristic of the reflected wave.

3. The effect of a rugged boundary

Any realistic deterministic description of a continental shelf, even if that description were available, would lead to a problem formulation so complex that the effort required to solve it could not be justified. Since we don't have such descriptions except in very coarse scale and since we could not handle them anyway, we adopt the following attitude (set of hypotheses).

(1) The fact that the shelf is sloping implies a reflected-wave profile, at each y, much like that derived in §2.

(2) The undulations in coastline have a further impact which can be *modelled* by a rule that says: the wave which would have arrived at $x = 1$ after reflection by a plane shelf actually does arrive there but with a time delay (or lead) 'implied' by the extent, locally, of the ragged boundary indentation (or projection) beyond the nominal coastline.

(3) The characterization of the undulation will be given stochastically in terms, not of the coastline geometry, but rather of its implied time-delay distribution.

Thus, in the deep water, we have

$$v_{xx} + v_{yy} - v_{\tau\tau} = 0, \tag{3.1}$$

where v, this time, is the seaward (x) component of particle velocity of the reflected wave only. The geometry is shown in figure 7.

The boundary condition states that

$$v(1, y, \tau) = B\left(y - \frac{\tau - 2\beta f(y)}{\cos\theta}\right), \tag{3.2}$$

where $B(y - \tau\sec\theta)$ is the wave that would have reflected from a plane beach, β is

$\cot\theta$ and $f(y)$ is a random variable which takes on the values of the time delay (lead) which, at normal incidence, would be implied by the indentation (projection) of the coastline at y. The probability density function for f is taken to be

$$\rho(f(y)) = \left(\frac{1}{2\pi l^2}\right)^{\frac{1}{2}} e^{-f^2/2l^2}. \tag{3.3}$$

The solution of (3.1) in $x > 1$, subject both to the boundary condition (3.2) and to the Sommerfeld radiation condition, can be written

$$v(x,y,\tau) = \int\int_{-\infty}^{\infty} B[\tau' \sec\theta - y' - 2\beta f(y')\sec\theta]\, K(\tau-\tau', x, y-y')\, d\tau'\, dy', \tag{3.4}$$

where K is that Green function about which we only need to know that

$$\int\int H(\tau' \sec\theta - y')\, K(\tau-\tau', x, y-y')\, d\tau'\, dy' \equiv H(\tau\sec\theta - y - \beta x). \tag{3.5}$$

In view of the crudeness of the model, no significant accuracy is lost when we approximate B as a sum of Gaussian functions of the form

$$B_n(y) = a_n e^{-y^2/2W_n^2},$$

and our objective is met when we carry out the analysis for one such B_n, i.e.

$$B = e^{-y^2/2W^2}. \tag{3.6}$$

For this choice of B, the ensemble average of v is given by

$$\begin{aligned}\langle v\rangle &= \int\int_{-\infty}^{\infty} d\tau'\, dy'\, K(\tau-\tau', x, y-y')\left\langle \exp\left[-\frac{[\tau'\sec\theta - y' - 2\beta\sec\theta f(y')]^2}{2W^2}\right]\right\rangle \\ &= \int\int_{-\infty}^{\infty} d\tau'\, dy'\, K(\tau-\tau', x, y-y')\frac{1}{\mu}B\left(\frac{\tau'\sec\theta - y'}{\mu}\right),\end{aligned} \tag{3.7}$$

where

$$\mu = \left(1 + \frac{4l^2}{W^2\sin^2\theta}\right)^{\frac{1}{2}}. \tag{3.8}$$

The final factor in (3.7) was obtained by evaluating

$$\left\langle \exp\left[-\frac{[\tau'\sec\theta - y' - 2bf(y')\sec\theta]^2}{2W^2}\right]\right\rangle$$

$$\equiv \int_{-\infty}^{\infty} \frac{1}{(2\pi l^2)^{\frac{1}{2}}} \exp\left[\frac{-f^2}{2l^2} - \frac{[\tau'\sec\theta - y' - 2\beta f(y')\sec\theta]^2}{2W^2}\right] df. \tag{3.9}$$

Thus, using the previously cited property (3.5) of the Green function, (3.7) implies that

$$\langle v(x,y,t)\rangle = \frac{1}{\mu}B\left(\frac{\tau\sec\theta - y}{\mu}\right). \tag{3.10}$$

That is to say, the ensemble average of the family of reflected waves duplicates the wave that would have reflected from the plane shelf except that the horizontal scale of that reflection has been broadened by the factor μ and the amplitude has been weakened by the same factor.

Unfortunately, the interpretation of this result varies according to information about the geometries $f(y)$ which is not contained in any of the foregoing. For example, if $f(y')$ were completely uncorrelated to $f(y'')$ for all $y'' \neq y'$, the excitation at $x = 1$ is

equivalent to one in which different partial masses of the water adjacent to $x = 1$ are acted on by 'pistons' according to differing values of f all in accord with the distribution (3.3). Under these circumstances, in each realization of the phenomenon, the radiated wave has the form given in (3.10). Conversely, if the autocorrelation of f is so far-reaching that $f(y') \equiv f(y'')$ for all y', y'', then each reflected wave is merely given by

$$v_{\mathrm{refl}}^{(n)} = B[\tau \sec\theta - y - 2\beta(x - f_n)\sec\theta], \tag{3.11}$$

where f_n is the value of f associated with the nth realization. Thus, in this case, the description (3.10) is an artifact of a set of waves having identical shapes and amplitudes appropriate to the plane shelf but with uncertainties in position which lead to (3.10).

In order to show that the appropriate interpretation is that *each* realization is broadened in accord with (3.10), we will investigate in §4 the waves associated with a particular family of deterministic rigged coastlines.

4. A useful deterministic coastline

One particular, simply described, discretized family of coastline realizations $f(y)$ is that in which the time delay f on one set of intervals $R^{(1)}$ has the value f_1, whereas, on the complementary set of intervals $R^{(2)}$, f takes on the value $f_2 = -f_1$.

The boundary-value problem that accompanies this special case is

$$v_{xx} + v_{yy} - v_{\tau\tau} = 0, \tag{4.1}$$

$$v(1, y, \tau) = B[\tau - f(y)], \tag{4.2}$$

where v must represent an outgoing wave. The absence of $\sec\theta$ in the argument of B indicates that, for this particular problem, we find it convenient and adequate to confine our attention to waves whose incidence is normal to the coastline.

With little further loss in generality we also confine our attention to cases in which the intervals in both $R^{(1)}$ and $R^{(2)}$ have length L, for which the boundary condition becomes

$$\begin{aligned} v(1, y, \tau) &= B[\tau - f_n(y)] \\ &= \mathrm{e}^{-(\tau - f_1)^2/2W^2} F_1(y) + \mathrm{e}^{-(\tau + f_1)^2/2W^2} F_2(y), \end{aligned} \tag{4.3}$$

where

$$\begin{aligned} F_1(y) &= \tfrac{1}{2} + \sum_{n=0}^{\infty} \frac{2}{(2n+1)\pi} \sin\frac{(2n+1)\pi y}{L}, \\ F_2(y) &= \tfrac{1}{2} - \sum_{n=0}^{\infty} \frac{2}{(2n+1)\pi} \sin\frac{(2n+1)\pi y}{L}. \end{aligned} \tag{4.4}$$

It is clear that the contribution of the constant terms in this boundary condition imply a result that is the direct counterpart of the ensemble average of (3.10),† and the remaining question is: at what offshore distance x (if any) does the contribution of the reflection from one or another of the trigonometric terms in (4.4) die off to negligible values? It is rather clear that the $n = 1$ case will decay most slowly, so we look at (4.1) subject to

$$v(1, y, \tau) = \sin\frac{\pi y}{L} B(\tau). \tag{4.5}$$

Equation (4.1) becomes, with $v(x, y, \tau) = \sin(\pi y/L)\,\rho(x, \tau)$,

$$\rho_{xx} - \rho_{\tau\tau} - \frac{\pi^2}{L^2}\rho = 0, \tag{4.6}$$

† It is even clearer when one imagines a boundary condition with 17 sets of intervals with 17 values of f.

and (4.5) becomes

$$\rho(1,\tau) = B(\tau) = \mathrm{e}^{-\tau^2/2W^2}. \tag{4.7}$$

Using the Fourier transform (in t) again, we obtain

$$\bar{\rho}_{xx} - \left(\frac{\pi^2}{L^2} - \xi^2\right)\bar{\rho} = 0, \tag{4.8}$$

with

$$\bar{\rho}(1,\xi) = B(\xi) = \mathrm{e}^{-\frac{1}{2}W^2\xi^2}. \tag{4.9}$$

The solution of this problem can be written

$$\bar{\rho}(x,\xi) = \exp\left[-\tfrac{1}{2}W^2\xi^2 - \left(\frac{\pi^2}{L^2} - \xi^2\right)^{\frac{1}{2}}(x-1)\right], \tag{4.10}$$

and the inversion is not elementary. However, we can ferret out the characteristic features of ρ in the following straightforward way.

Suppose first that L is less than or equal to W and note that (a) most of the energy (or momentum, ...) is associated with wavenumbers ξ which lie in $0 < \xi < 2/L$, and (b) $\bar{\rho}$ decays with x at least as rapidly as $\mathrm{e}^{-\sqrt{6}(x-1)/L}$ for that range of ξ.† That is to say: by the time the reflected pulse has travelled seaward a few distances L most of the energy in the wave has disappeared via 'destructive interference', and only the small-wavelength contribution remains. Within the framework of the foregoing theory, these spectral components of the wave could still imply some strong gradients in ρ, but, in fact, the waves in this spectral range are the ones that disperse strongly in the more properly formulated problem, and, if the dispersive theory were called upon, *no* significant consequences of these wavy inputs would remain. Conversely, of course, if the coast has a ragged boundary in small scale (i.e. $O(W)$) superposed on an undulation at a scale L_2 that is considerably larger than W the consequences of that geometry will include a wavy locus with lateral scale L_2 for the reflected wave we have just described.

Accordingly, one can expect the reflection from a real shelf to have a waviness in location whose details we don't care about but which are strongly correlated with the large-scale undulations in coastline position. One can also expect that reflection to have a profile which, except for an amplitude diminution and a broadening μ, is that given by the analysis of §2 as depicted in figures 2–6. The diminution and broadening which will have occurred in only a few seaward distances W will be characterized by μ ((3.8) and (3.10)), with l chosen to represent the mean delay time associated with the stochastic irregularities whose scales s (in y) lie in $0 < s \leqslant O(W)$.

And, finally, since $W < 0.2$ for real tsunamis, the reflected tsunami will have a much greater breadth and less than half the amplitude of the incident wave.

Appendix A

The explicit form of the inversion integral for the shelf solution $\eta(x,s)$ is

$$\eta(x,s) = \frac{w}{\pi^{\frac{1}{2}}\cos\theta}\int_{-\infty}^{+\infty} \mathrm{d}\xi\left[\frac{M(a,1,2\xi x)\,\mathrm{e}^{-\xi(x-1)}}{\chi}\right]\frac{\exp\left[-\left(\frac{\xi w}{2\cos\theta}\right)^2 + \mathrm{i}\xi s - \mathrm{i}\xi\tan\theta\right]}{1+\mathrm{i}\left(\frac{\psi}{\chi}\right)\cot\theta}, \tag{A 1}$$

† A more formal verification of this exponential decay for the long wavelengths is given by Watson's lemma, which yields the estimate $\approx \mathrm{e}^{-\pi(x-1)/L}$, i.e. (4.10) with $\xi = 0$.

where

$$\psi \equiv M(a,1,2\xi)-(1+\gamma^2\xi)\,M(a,2,2\xi),$$

$$\chi \equiv M(a,1,2\xi), \quad a=\tfrac{1}{2}(1-\xi\gamma^2).$$

The integral is cast in real form by first making repeated use of Kummer's relation (Abramowitz & Stegun 1965)

$$M(\alpha,\gamma,z) = \mathrm{e}^z M(\gamma-\alpha,\gamma,-z),$$

and known recurrence formulas for the M-function, to establish that

$$P(\xi) \equiv \frac{M(a,1,2\xi x)\,\mathrm{e}^{-\xi(x-1)}}{M(a,1,2\xi)} = P(-\xi),$$

$$R(\xi) \equiv \frac{\psi(\xi)}{\chi(\xi)} = -R(-\xi).$$

With these symmetry relations, (A 1) can be written

$$\eta(x,y) = \frac{2w}{\pi^{\frac{1}{2}}}\int_0^\infty \mathrm{d}\xi\,\mathrm{e}^{-\xi(x-1)}\,\hat{M}(a,1,2\xi x)\exp\left[-\left(\frac{\xi w}{2\cos\theta}\right)^2\left[\frac{\left[\hat{M}\dfrac{\cos\xi y}{\cos\theta}+\hat{\psi}\dfrac{\sin\xi y}{\sin\theta}\right]}{\hat{M}^2+\hat{\psi}^2\cot^2\theta}\right]\right], \tag{A 2}$$

where $\hat{M} = \mathrm{e}^{-\xi}M(a,1,2\xi)$, $\hat{\psi} = \mathrm{e}^{-\xi}\psi$, and a value of t has been chosen in (A 2) so that the crest of the incident wave passes through $x=1$, $y=0$. The $\hat{M}$- and $\hat{\psi}$-functions are evaluated (in ξ) by using either the series representation together with recurrence relations on M, or finite-domain integral representations. Though for large ξ the intergrand is a rather rapidly oscillating (and decaying) function, the standard quadrature routines provide sufficient accuracy.

One feature of the solution, which served as a mild check of the numerics, follows from the expressions (2.8), (2.13) and the Fourier-transform relation

$$\bar{g}(0) = \int_{-\infty}^{+\infty} \mathrm{d}y\,g(y).$$

By evaluating (2.8) with $\xi = 0$, it follows immediately that the integral in y, for some $x_0 > 1$, of the incident and reflected wave is equal to $2\bar{A}(0)$, or $2w\pi^{\frac{1}{2}}/\cos\theta$. Though somewhat less easily established, it is also true that

$$\int_{-\infty}^{+\infty} \eta(x_0 \leqslant 1, y)\,\mathrm{d}y = \frac{2w\pi^{\frac{1}{2}}}{\cos\theta}.$$

The numerical values generated by (A 2) for $x = 0, \frac{1}{2}, 1$ were integrated (in y) to ensure that this condition was satisfied with acceptable accuracy.

Appendix B

The formalism outlined in §2 may be used to derive explicit expressions for the waveform when the underlying geometry consists of a constant depth $\mu^2 h_0$ ($\mu^2 < 1$) in $0 < x < 1$ and deep water (h_0) in $x > 1$. No change is required in the $\phi(x)$ solution (2.8), and the appropriate counterpart to (2.7) is given by

$$\bar{\eta}_{xx}(x,\xi) - (r\xi)^2\,\bar{\eta}(x,\xi) = 0,$$

$$r = \frac{(1-\mu^2\cos^2\theta)^{\frac{1}{2}}}{\mu\cos\theta}.$$

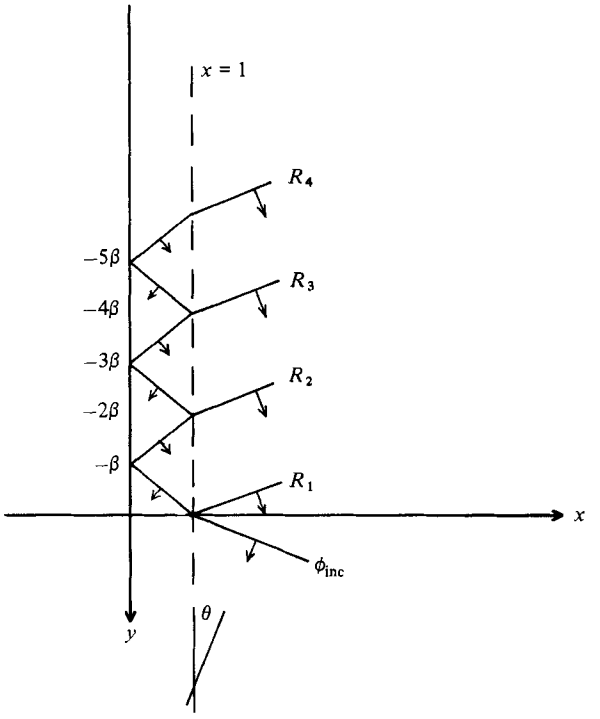

FIGURE 8. Schematic diagram of the level line distribution for the step-shelf geometry.

Imposing the boundary condition $\bar{\eta}_x(0,\xi) = 0$ at the 'coastline', together with the matching criteria

$$\bar{\eta}(1,\xi) = \bar{\phi}(1,\xi),$$

$$\mu^2\bar{\eta}_x(1,\xi) = \bar{\phi}_x(1,\xi)$$

at the edge of the shelf, uniquely determines the reflection coefficient, now given by

$$\frac{\bar{B}(\xi)}{\bar{A}(\xi)} = \frac{\cos(\xi r)+iQ\sin(\xi r)}{\cos(\xi r)-iQ\sin(\xi r)}, \tag{B 1}$$

where

$$Q = \frac{\mu(1-\mu^2\cos^2\theta)^{\frac{1}{2}}}{\sin\theta}.$$

The transformed waveheights

$$\bar{\eta}(x,\xi) = \frac{\cos(\xi r x)}{\cos(\xi r)}\bar{A}(\xi)\left(1+\frac{\bar{B}(\xi)}{\bar{A}(\xi)}\right), \tag{B 2}$$

$$\bar{\phi}(x,\xi) = \bar{A}(\xi)\left[e^{-i\xi\tan\theta(x-1)} + \frac{\bar{B}(\xi)}{\bar{A}(\xi)}e^{i\xi\tan\theta(x-1)}\right] \tag{B 3}$$

can be inverted explicitly when $\bar{B}/\bar{A}$ is written as a power series in $e^{i\xi r}$. The reflection coefficient may be cast as a sum:

$$\frac{\bar{B}(\xi)}{\bar{A}(\xi)} = \delta + (1-\delta^2)\sum_{n=1}^{\infty}(-\delta)^{n-1}e^{2ni\xi r}, \tag{B 4}$$

where $\delta \equiv (1-Q)/(1+Q)$ is the reflection coefficient associated with normal incidence on a step change in depth. The 'effective' depth difference $1-Q^2$, however, is now determined by the height μ^2 of the step and the obliquity θ of the incident wave.

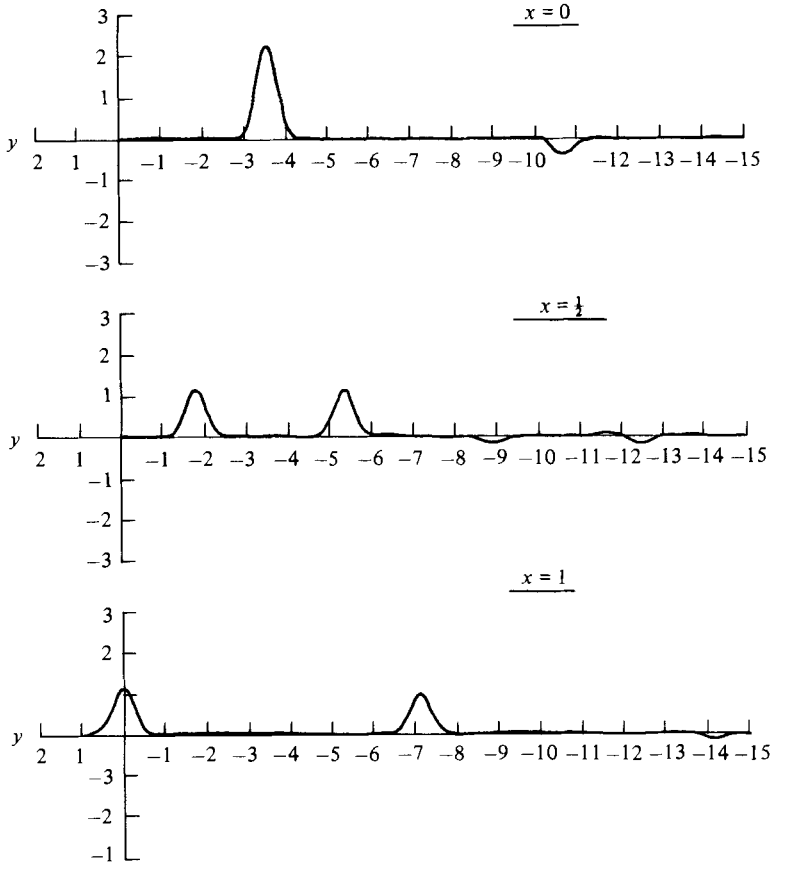

FIGURE 9. Wave profiles on the step shelf with $\mu^2 = 0.5$, $w = 0.25$ and $\theta = \frac{3}{8}\pi$.

Inverting the transforms $\bar{\eta}$ and $\bar{\phi}$ using (B 4) provides infinite-series expressions for $\eta(x, s)$ and $\phi(x, s)$. With the same incident waveform $A(\lambda)$ as before, the solutions

$$\eta(x,s) = (1+\delta)\sum_{m=0}^{\infty}(-\delta)^m\left[\exp-\left\{\frac{\cos^2\theta}{w^2}[rx-F]^2\right\}+\exp\left\{-\frac{\cos^2\theta}{w^2}[rx+F]^2\right\}\right], \tag{B 5}$$

where $F = 2r(m+\frac{1}{2})-\tan\theta+s$,

$$\phi(x,s) = \phi_{\text{inc}}(x,s)+\delta\exp\left[-\frac{\cos\theta^2}{w^2}G^2\right] + (1-\delta^2)\sum_{m=1}^{\infty}(-\delta)^{m-1}\exp\left[-\frac{\cos^2\theta}{w^2}(G+2mr)^2\right],$$

where $G = (x-2)\tan\theta+s$, represent a collection of plane Gaussian pulses whose (maximum) level lines combine in the manner shown in figure 8.

The shelf solution $\eta(x, s)$ was evaluated numerically using the incident wave shapes described in §2, and figure 9, where $\mu^2 = 0.5$, $w = 0.25$ and $\theta = \frac{3}{8}\pi$, is typical among the results that emerged. No shelf-height and incident-angle combination provided either the degree of amplification or the dipole character found to prevail in the solutions for the sloping shelf.

REFERENCES

ABRAMOWITZ, M. & STEGUN, L. A. (eds.) 1965 *Handbook of Mathematical Functions*. Nat. Bureau of Standards.

CARRIER, G. F. 1971 Dynamics of tsunamis. In *Mathematical Problems in the Geophysical Sciences - Vol. 1 - Geophysical Fluid Dynamics* (ed. W. H. Reid). American Mathematical Society.